Large-Signal HBT Characterization and Modeling at Millimeter Wave Frequencies

Douglas A. Teeter, *Member, IEEE,* Jack R. East, *Member, IEEE,* and George I. Haddad, *Fellow, IEEE*

Abstract—**This paper presents a detailed large-signal analysis for the heterojunction bipolar transistor. Using a combination of computer models and corrected measurements, we have analyzed the bias and frequency dependence of the gain compression from 8 to 35 GHz for several HBT's. From 8 to 16 GHz, a commercial tuner system was used for making the measurements. However, beyond 26 GHz, an active load pull system was designed and constructed to circumvent problems created by component losses. Several comparisons between measured and modeled data are provided to illustrate the effectiveness of the characterization technique.**

I. Introduction

OVER the past decade, the frequency and power performance of the heterojunction bipolar transistor (HBT) has improved dramatically. While f_T's and f_{max}'s of only a few gigahertz were possible in the early 1980's [1], f_T values exceeding 50 GHz and f_{max} values above 100 GHz are not uncommon [2], [3]. Rapid improvements in material quality and fabrication techniques have made such progress possible.

This improved frequency performance has made HBT circuit designs in Ku and Ka band achievable. Amplifiers with 30 GHz of bandwidth have been reported [4], and voltage controlled oscillators covering 25–42 GHz (with two separate oscillator circuits) have been built [5]. As the operating frequency increases, accurate high-frequency device characterization and modeling becomes more significant. Vector error correction techniques are more important at higher frequencies where measurement system components are usually far from ideal. In terms of modeling, transit time delays become more significant at higher frequencies. Many commonly used models, such as the Gummel Poon model, lose accuracy in the millimeter wave regime because they neglect this effect [6].

We address these issues in this paper by presenting measured and modeled large-signal results for a typical HBT at several bias points from 8 to 35 GHz. A commercial tuner system was used to perform the measurements from 8 to 16 GHz. To collect data from 27 to 35 GHZ, however, an active load pull system was designed and constructed. This system is described, and a brief description of the error correction approach is given. To help explain the measured results, a modified Ebers–Moll model was developed [6]. Using both measured and simulated results, we have investigated the frequency dependence of the gain compression at several bias points. It is shown that simple load line techniques can be applied at millimeter wave frequencies as long as the analysis is performed on the intrinsic device and transit time delays are included in the calculations.

This work was supported by the U.S. Army Research Office under the URI program, Grant DAAL03-92-G-0109. Manuscript received May 18, 1992; revised November 2, 1992. This work was presented in part at the 37th ARFTG Conference, Boston, MA, June 1991.

D. A. Teeter was with the Department of Electrical Engineering and Computer Science, University of Michigan, Ann Arbor, MI. He is now with Raytheon Company, Lexington, MA 02173.

J. R. East and G. I. Haddad are with the Department of Electrical Engineering and Computer Science, University of Michigan, Ann Arbor, MI 48109-212..

IEEE Log Number 9209338.

II. Measurement Systems

The large-signal measurements consisted of presenting a known load and source impedance to the transistor at a given frequency and then measuring the associated input power, output power, and dc bias conditions. In order to cover a wide frequency range (8–35 GHz), two separate measurement systems were used. At lower frequencies (8–16 GHz), a commercial computer controlled tuner system (Focus Microwaves [7]) was used to vary the load impedance, as illustrated in Fig. 1. The RF source consisted of a synthesized signal generator, a solid state amplifier, and an isolator to create a nominal 50 Ω source impedance. Input power levels were detected using a directional coupler. On the output, a coaxial electromechanical tuner was used to control the load impedance. Since the system was coaxial, the output bias network could be placed behind the tuner, thereby reducing losses between the tuner and the transistor terminals. This low loss signal path made it possible to present the device with high VSWR loads. To protect the output power detector, a 10 dB attenuator was placed in front of the power head. Data acquisition and tuner control were automated using an external computer.

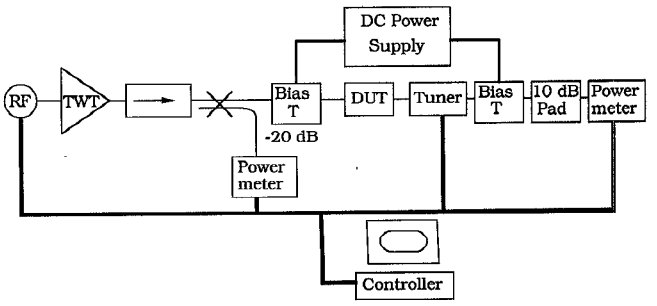

Fig. 1. Commercial passive tuner system used for 8–16 GHz power measurements.

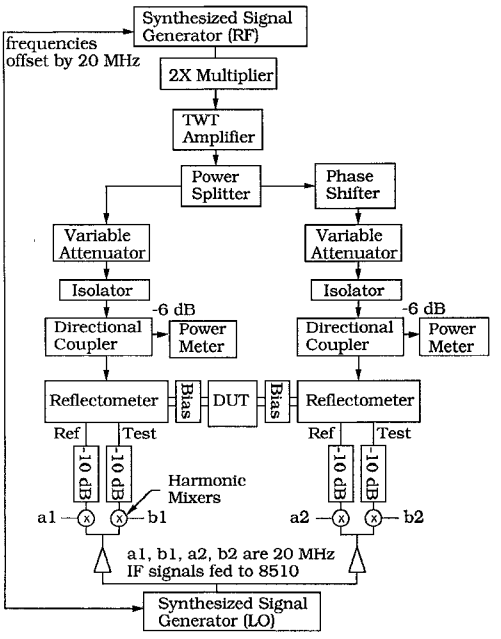

Fig. 2. Active load pull system used for 27–35 GHz power measurements.

Above 26 GHz, only waveguide components were available. Using waveguide, however, forced us to place the bias tees in the signal path between the tuner and the transistor (refer to Fig. 2). The insertion loss of the commercial bias tees we were using (more than 1.5 dB above 27 GHz) severely limited the tuning range of our passive tuners at millimeter wave frequencies. To circumvent this problem, we constructed an active load pull system based on the principles found in [8] and [9]. Our system was first described in [10], and overall improvements along with error correction techniques were presented in [11] and [12]. In this paper, we merely highlight some of the key points before giving some measured results.

A complete block diagram of the system is given in Fig. 2. By varying the magnitude and phase of the incident signal at port 2 with respect to the incident signal at port 1, one can electronically impose any load impedance on the DUT [9]. Furthermore, since the load is actively generated, one can compensate for system losses by increasing the magnitude of the active reflection signal. The signal source consisted of a synthesized signal generator (13–20 GHz), a millimeter wave doubler, and a 26–40 GHz TWT amplifier. The output of the TWT was split to create an incident signal at port 1 and 2. By using variable attenuators and phase shifters, the magnitude and phase of the actively reflected signal could be controlled. Isolators on both the input and output signal paths were used to separate VSWR changes due to varying the attenuators and phase shifters from the main part of the measurement system. Input and output power levels were measured using directional couplers. To measure the reflection coefficients, reflectometers consisting of back-to-back directional couplers were used. The raw incident and reflected signals were detected using harmonic mixers with an IF frequency of 20 MHz. These 20 MHz signals were then fed into an HP 8510B network analyzer so that the load and input impedance could be measured in real time. To keep the mixers operating in the linear region, attenuators were used. For our application, 10–20 dB of attenuation was adequate.

In order to achieve maximum accuracy, all the measurements made with our active load pull system were vector corrected. An external computer was used to calculate and apply the necessary correction to the power levels. The basic equations used for correcting our measurements were developed in [13], and a complete presentation of our error correction techniques was given in [11] and [12].

This measurement system has been used to study gain compression and optimum load shift at millimeter wave frequencies. In the next section, we describe a simple model which was used in connection with measured results to help explain the frequency and V_{ce} dependence of the 1 dB compression point.

III. Modeling

Using a detailed numerical simulator which includes velocity overshoot and energy relaxation effects, we have developed a simple Ebers–Moll model which includes transit time effects [6]. A brief summary of the model described in [6] will be presented here. The active portion of this model is given in Fig. 3. To include parasitic effects, the active device was placed in the circuit depicted in Fig. 4. The corresponding model parameters, obtained from dc and multibias S-parameter measurements, are given in Tables I and II. Our model is similar to a small-signal HBT model developed by Maas *et al.* [14], except that we include a diode modeling the

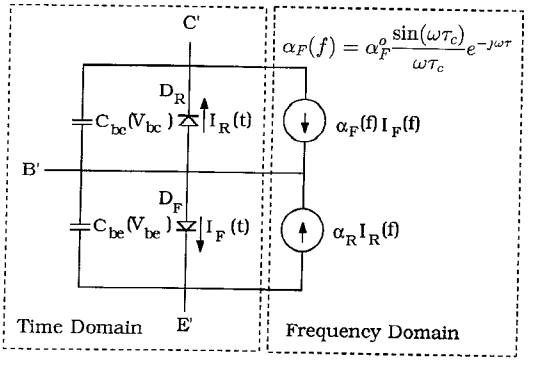

Fig. 3. Large-signal active portion of the Ebers–Moll model.

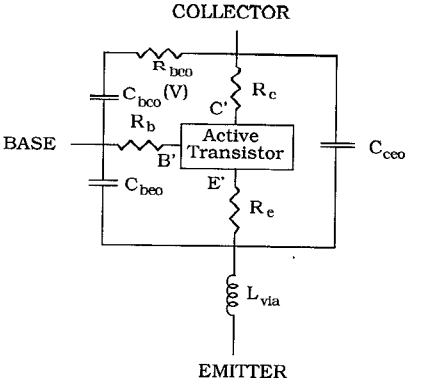

Fig. 4. Parasitic circuit which the active device models are embedded in. Elements values are given in Table II.

TABLE I
MODEL PARAMETERS

Parameter	Value	Description
α_F^o	0.94	Common base current gain—forward direction
α_R	$4.56 \cdot 10^{-4}$	Common base current gain—reverse direction
τ	1.7–3.1 ps	Forward transit time delay in I_c
I_{ss}	$6.95 \cdot 10^{-26}$ A	Saturation current $(I_{ss} = \alpha_F^o I_{sF} = \alpha_R I_{sR})$
I_{sF}	$7.39 \cdot 10^{-26}$ A	Forward saturation current
I_{sR}	$1.52 \cdot 10^{-22}$ A	Reverse saturation current
n_F	1.07	Base emitter junction ideality factor
n_R	1.00	Base collector junction ideality factor
C_{jeo}	180 fF	Zero bias base-emitter junction capacitance
V_{jeo}	1.64 V	Base-emitter junction built in potential
M_{je}	0.5	Base-emitter junction grading coefficient
τ_F	1.03 pS	Diffusion time (C_{be}^{diff})
C_{jco}	34 fF	Zero bias base-collector junction capacitance
V_{jco}	1.42 V	Base-collector junction built in potential
M_{jc}	0.5	Base-collector junction grading coefficient

Note: α_F^o is the low-frequency value of α_F; α_R is assumed frequency independent.

TABLE II
PARASITICS $I_c = 18$ mA, $V_{ce} = 2$ V

Component	Value	Description
C_{bco}	50 fF	Extrinsic base-collector capacitance
C_{beo}	45 fF	Base-emitter interconnect capacitance
C_{ceo}	71 fF	Collector-emitter interconnect capacitance
L_{via}	14.5 pH	Emitter via hole inductance
R_{bco}	2.1 Ω	Extrinsic collector access resitance
R_b	15.6 Ω	Base resistance
R_c	6.8 Ω	Collector resistance
R_e	2.1 Ω	Emitter resistance

base-collector junction, D_R, and a current generator, $\alpha_R I_R$, modeling reverse injection into the emitter. These components play an insignificant role under the conditions considered in [14], small-signal active region, but can be very important for large-signal calculations where the RF collector voltage swing may forward bias the base-collector junction over part of the RF cycle. Our model is also similar to that reported by Grossman and Choma [15], except that we use a harmonic balance technique [16] rather than an exclusive time domain method to perform our simulations.

Transit time delays were implemented in the frequency domain through the frequency dependence of the forward current gain,

$$\alpha_F(f) = \alpha_F^o \frac{\sin(\omega\tau_c)}{\omega\tau_c} e^{-j\omega\tau} \tag{1}$$

as illustrated in Fig. 3. Since the collector transit time τ_c accounted for at least 90% of the forward transit time delay τ, little error resulted by substituting τ for τ_c in (1). Calculations of voltages and currents for the nonlinear diodes and capacitors were made in the time domain, while the injection current generators were implemented in the frequency domain. The two domains were linked using the LIBRA harmonic balance software [17].

As explained in [6], the conduction currents were modeled as

$$I_F = I_{sF}\left(\exp\left[\frac{qV_{be}}{n_F kT}\right] - 1\right) \tag{2}$$

$$I_R = I_{sR}\left(\exp\left[\frac{qV_{bc}}{n_R kT}\right] - 1\right) \tag{3}$$

where

$$I_{ss} = \alpha_F^o I_{sF} = \alpha_R I_{sR}\,. \tag{4}$$

Definitions and typical values for the parameters used in these equations are given in Table I. I_F represents the sum of electron and hole *injection* current across the emitter junction. Recombination components, which primarily affect the base current, were included in the model by making the low-frequency forward current gain α_F^o dependent on V_{be}. During microwave RF simulations, the variation in the instantaneous V_{be} causes α_F^o to fluctuate about its small-signal value. However, because the RF variation in V_{be} is usually small (less than 0.1 V for the bias points and power levels studied in this paper), good agreement with measured data was achieved by simply using a constant α_F^o whose value was extracted from small-signal data at the dc quiescent bias point of interest. This simplification includes the dc component of the recombination current, but it neglects any RF variation. At millimeter wave

frequencies, however, the transit time delay between collector and emitter current dominates the base current more than the variation in α_F° and, hence, the recombination current.

Junction capacitances were modeled using simple depletion and diffusion equations. The base emitter capacitance was modeled with both a diffusion and a depletion component using

$$C_{be} = C_{je} + C_{diff} \tag{5}$$

$$= C_{jeo}\left(1 - \frac{V_{be}}{V_{je}}\right)^{-M_{je}} + \frac{qI_F\tau_F}{kTn_F}. \tag{6}$$

Only a depletion component was used to model the base collector capacitance since this junction was not strongly forward biased except under very high gain compression operation. Thus, C_{bc} was written as

$$C_{bc} = C_{jco}\left(1 - \frac{V_{bc}}{V_{jc}}\right)^{-M_{jc}}. \tag{7}$$

Both the emitter and collector junction grading coefficients, M_{je} and M_{jc}, were assumed to be 0.5 because the devices were fabricated on MOCVD grown material, a growth technique known to produce highly abrupt metallurgical junctions. The remaining parameters in (6) and (7)—C_{jeo}, V_{je}, τ_F, C_{jco}, and V_{jc}—were obtained by equivalent circuit fitting to multibias S-parameter measurements.

IV. Results

By using both measured and modeled data, we were able to perform a detailed study of the frequency and bias dependence of gain compression. The model was used to help guide and explain the measured results. Despite the simplicity of the model, excellent agreement between measured and modeled data has been obtained.

All the measurements presented in this paper were made on two finger, 2×20 μm^2 emitter area GaAs/AlGaAs HBT's. The corresponding device structure is given in Table III. These smaller devices were used because the device impedance was not as close to the edge of the Smith Chart, thereby allowing a more accurate measurement. Measurement accuracy decreases as the impedance moves toward the edge of the Smith Chart [10]. Also, smaller area devices required less input power before gain compression occurred.

Measured and simulated input and output power at 1 dB power gain compression was compared for several class A bias points using small-signal conjugate match loading. The agreement at several collector voltages, shown in Figs. 5 and 6, is excellent. A corresponding plot of the power transfer characteristic and power added efficiency at 29.5 GHZ is given in Fig. 7. While the model is suitable for simulations in all regions of operation, ambiguities in the harmonic loading during the measurements made comparison to experimental data difficult for class B and C operating points. Therefore, to allow easy comparison to the measured data, only class A points were considered in this paper.

TABLE III
Structure of Measured Device (2 Finger, 2×20 μm Emitter Stripe)

Region	Al frac	dop	dop (cm^{-3})	μm
Contact	0.0	n+	$2 \cdot 17^{18}$	0.15
Grading	0.0–0.3	n+	$1 \cdot 10^{18}$	0.05
Emitter	0.3	n	$1 \cdot 10^{17}$	0.05
Base	0.	p+	$2 \cdot 10^{19}$	0.1
Collector	0.	n	$1 \cdot 10^{16}$	0.8
Subcollector	0.	n+	$2 \cdot 10^{18}$	1.5

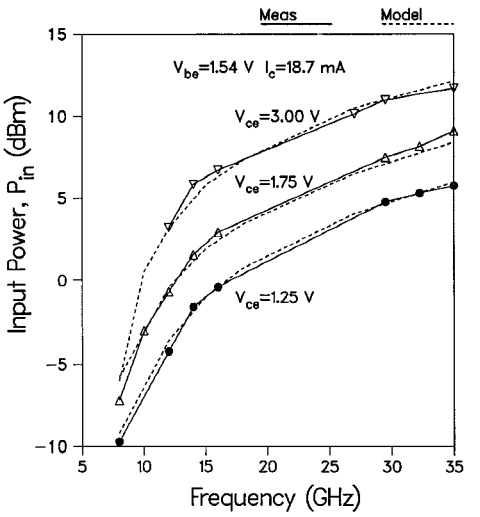

Fig. 5. Frequency and V_{ce} dependence of the input power (not *incident* power) at 1 dB power gain compression. Small-signal conjugate match loads were used on the output at each frequency.

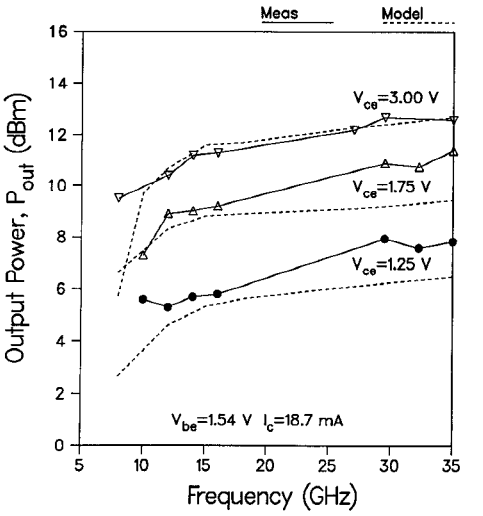

Fig. 6. Frequency and V_{ce} dependence of the output power at 1 dB power gain compression. Small-signal conjugate match loads were used on the output at each frequency.

Two nominally equivalent devices were used in this work. The main difference between the devices was the parasitics. The device used in the measurements for $V_{ce} = 1.25$ V and for $V_{ce} = 1.75$ V had parasitic values given in Table II. The second device, used in the measurements at $V_{ce} = 3$ V, had approximately the same parasitics except $R_b = 37$ Ω and $R_e = 7.3$ Ω. The better agreement between measured and modeled results for $V_{ce} = 3$ V is most likely due to a slightly better extraction of the parasitics for the second device.

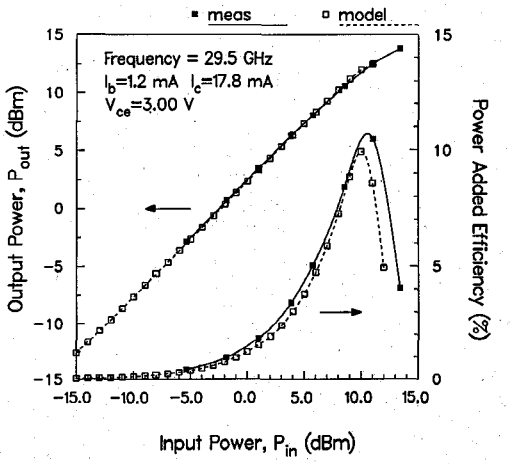

Fig. 7. Power transfer characteristic and power added efficiency at 29.5 GHz for $I_c = 17.8$ mA and $V_{ce} = 3$ V. $Z_L = 10.3 + j40.9\ \Omega$ and $Z_S = 15.5 + j4.4\ \Omega$ (small-signal optimum).

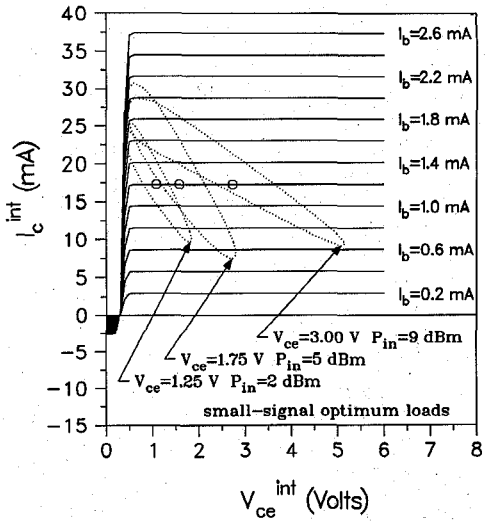

Fig. 8. Intrinsic load contours at 27 GHz for small-signal conjugate match loads with $V_{ce} = 1.25-3$ V and $I_c = 17.8$ mA. Dots in the figure correspond to the quiescent intrinsic dc bias points used during the calculations. The input power level for each contour correspond to the onset of gain compression for the respective collector voltage.

As can be seen in Figs. 5 and 6, when the frequency is increased, the input power necessary to compress the power gain increased because the maximum available gain decreased. Under small-signal conjugate match conditions, gain compression was caused by the device collector voltage swinging into the saturation or ohmic region of the *intrinsic* device (terminals B', C' and E' in Figs. 3 and 4). This is clearly illustrated by the simulated 27 GHz result in Fig. 8 which shows the intrinsic current versus voltage trajectory under large-signal operation with an input power just prior to gain compression. To compute this result, the time dependent collector voltage and current waveforms were first calculated using the harmonic balance method [16]. Intrinsic collector voltage and current pairs at each time step were then plotted against the intrinsic HBT I–V curves, resulting in Fig. 8. The slight oval shape of the contour is caused by a small reactive component in the intrinsic load.

Due to extensive feedback through the parasitic elements, the extrinsic load presented to the accessible base, collector, and emitter terminals of the HBT differed drastically from the intrinsic load seen at terminals B', C', and E' in Figs. 3 and 4. Therefore, in order to effectively analyze the gain compression at millimeter wave frequencies, a load line analysis can still be used, but it must be applied to the terminals of the intrinsic device since it is the nonlinear active portion of a transistor which is responsible for the gain compression. Also, transit time effects must be included in the calculation at millimeter wave frequencies since these delays represent a significant fraction of the RF cycle. Utilizing the intrinsic load line information, we notice that as the collector voltage increased from 1.25 to 3 V, the input and output power at 1 dB gain compression increased because the collector voltage swing became larger before clipping in the saturation region, as shown in Fig. 8.

The output power at 1 dB gain compression was almost frequency independent under small-signal conjugate match conditions for frequencies above 15 GHz. At X-band frequencies (8–12 GHz) and below, we noticed a slight decreased in the output power. Results from our model indicate that this frequency variation depended on the values of the parasitic elements.

The load for peak power differs significantly from the small-signal optimum value in many power applications. Fig. 9 shows the shift in optimum terminations as the power into the HBT increased. At each power level, the input power was held constant and the load was varied until maximum output power was measured. The optimum load and source impedance for each power level was then plotted on a Smith Chart, as shown in Fig. 9. Due to limitations in the available power from the measurement system, a low value of V_{ce} was used so the device could be driven further into compression. The cause of this shift can be best explained by performing a simple load line analysis on the intrinsic device terminals. Fig. 10 shows the intrinsic RF load line computed from our model. Under small-signal conditions, the optimum load is that which provides maximum power transfer, i.e., a conjugate match. Under higher power conditions, the optimum load is

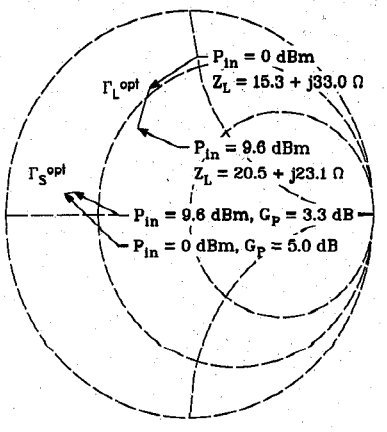

Fig. 9. Shift in load for maximum output power at 27 GHz as the input power increases. The corresponding intrinsic load contours, calculated from the Ebers–Moll model, are shown in Fig. 10; dc bias was $I_C = 17.8$ mA, and $V_{ce} = 1.75$ V.

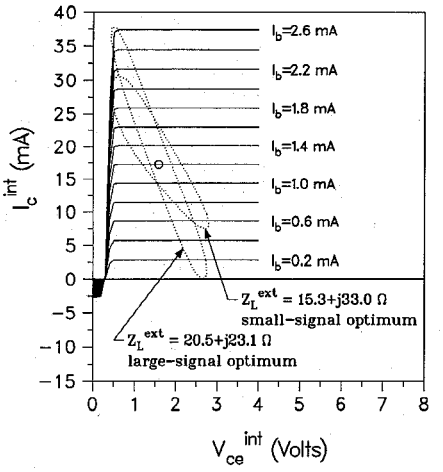

Fig. 10. Optimum intrinsic load contours under small-signal (P_{in} = 0 dBm) and large-signal (P_{in} = 9.6 dBm) operation at 27 GHz. The extrinsic loads correspond to the measured optimum values shown in Fig. 9; dc bias was I_c = 17.8 mA, and V_{ce} = 1.75 V.

that which provides the maximum intrinsic collector voltage and current swing before clipping in the saturation or cutoff regions.

As illustrated in the analysis just described, the load pull measurements and modified Ebers–Moll model serve as a valuable tool useful for understanding the large-signal operation of the HBT at millimeter wave frequencies. Due to its simplicity, the model can be easily incorporated into circuit simulations without excessive computational cost. This makes the model appealing for power amplifier and oscillator design in Ka bands and beyond, where transit time delays become significant.

V. Conclusions

Two different measurement systems, used for power measurements of HBT's, were described. From 8 to 16 GHz, a passive tuner system was used. Unfortunately, system losses restricted the tuning range of the passive tuners at millimeter wave frequencies. To achieve high VSWR loads above 27 GHz, an active tuning method was used. Details of the measurement technique and error correction were given. Vector correction was found to play a key role in improving measurement accuracy at millimeter wave frequencies.

Using the measurement systems, the frequency and bias dependence of the 1 dB gain compression point was analyzed. A modified Ebers–Moll model that includes transit time effects was used to assist in explaining the experimental results. It was shown that the conventional load line technique could still be applied at millimeter wave frequencies as long as one referred the analysis to the intrinsic device terminals and included transit time delay in the calculations. The measurement and modeling techniques described in this paper have direct application to high-frequency HBT amplifier and oscillator design.

Acknowledgment

The authors would like to thank Dr. A. Khatibzadeh from Texas Instruments, Central Research Laboratories; M. Afendykiw from the Naval Weapons Center; and Dr. B. Bayraktaroglu for providing us with HBT's to characterize. HBT development at Texas Instruments is being supported by the Naval Weapons Center, China Lake, CA, under Contract N-60530-89–C-0300. We would also like to thank D. Pehlke and J. Cowles from the University of Michigan for helpful discussions regarding this work.

References

[1] H. Beneking and L. M. Su, "GaAlAs/GaAs heterojunction microwave bipolar transistor," *Electron. Lett.*, vol. 17, pp. 301–302, Apr. 16, 1981.
[2] N. H. Sheng, M. F. Chang, P. M. Asbeck, K. C. Wang, G. J. Sullivan, D. L. Miller, J. A. Higgins, and E. Sovero, "Highpower GaAlAs/GaAs HBTs for microwave applications," in *IEEE IEDM Dig.*, 1987, pp. 619–622.
[3] N. L. Wang, N. H. Sheng, W. J. Ho, M. F. Chang, G. J. Sullivan, J. A. Higgins, and P. M. Asbeck "18 GHz high gain, high efficiency power operation of AlGaAs/GaAs HBT," in *IEEE MTT-S Dig.*, 1990, pp. 997–1000.
[4] N. H. Sheng, W. J. Ho, N. L. Wang, R. L. Pierson, P. M. Asbeck, and W. L. Edwards, "A 30 GHz bandwidth AlGaAs–GaAs HBT direct-coupled feedback amplifier," *IEEE Microwave Guided Wave Lett.*, vol. 1, pp. 208–210, Aug. 1991.
[5] D. M. Smith, J. C. Canyon, and D. L. Tait, "25–42 GHz GaAs heterojunction bipolar transistor low phase noise push-push VCO's," in *IEEE MTT-S Dig.*, 1989, pp. 725–728.
[6] D. A. Teeter, J. R. East, R. K. Mains, and G. I. Haddad, "Large-signal numerical and analytical HBT models," *IEEE Trans. Electron Devices*, May 1993, pp. 837–845.
[7] C. Tsironis, "A computer controlled tuner for accurate oscillator load pull measurements," *Microwave J.*, pp. 314–316, May 1991.
[8] D. C. Yang and D. F. Peterson, "Large-signal characterization of two-port nonlinear active networks," in *IEEE MTT-S Dig.*, 1982, pp. 345–347.
[9] R. Actis and R. A. McMorran, "Millimeter load pull measurements," *Appl. Microwave*, pp. 91–102, Nov./Dec. 1989.
[10] D. A. Teeter, J. R. East, R. K. Mains, and G. I. Haddad, "Large signal characterization and numerical modeling of the GaAs/AlGaAs HBT," in *IEEE MTT-S Dig.*, 1991, pp. 651–654.
[11] D. A. Teeter, J. R. East, and G. I. Haddad, "Error correction and power calibration of active load pull measurement systems," in *Proc. 37th ARFTG Conf.*, pp. 86–93, June 1991.
[12] D. A. Teeter, "Large-signal characterization and modeling of the heterojunction bipolar transistor," Ph.D. dissertation, University of Michigan, 1992.
[13] R. S. Tucker and P. D. Bradley, "Computer-aided error correction of large-signal load-pull measurements," *IEEE Trans. Microwave Theory Tech.*, vol. MTT-32, pp. 296–300, Mar. 1984.
[14] S. A. Maas, B. L. Nelson, and D. L. Tait, "Intermodulation in heterojunction bipolar transistors," *IEEE Trans. Microwave Theory Tech.*, vol. 40, pp. 442–448, Mar. 1992.
[15] P. Grossman and J. Choma, "Large-signal modeling of HBT's including self-heating and transit time effects," *IEEE Trans. Microwave Theory Tech.*, vol. 40, pp. 449–464, Mar. 1992.
[16] S. A. Maas, *Nonlinear Microwave Circuits.* Norwood, MA: Artech House, 1988, pp. 81–153.
[17] *Libra Users Guide*, EESOF, 5601 Lindero Canyon Road, Westlake Village, CA 91362.

Douglas A. Teeter was born in Richmond, VA, in 1964. He received the B.S.(EE) degree in 1987 from the Virginia Polytechnic Institute and State University, Blacksburg, and the M.S.(EE) and Ph.D.(EE) degrees from the University of Michigan, Ann Arbor, in 1988 and 1992, respectively.

From 1987 to 1992 he worked as a Research Assistant at the Center for High-Frequency Microelectronics at the University of Michigan. Currently he is a Senior Scientist at the Research Division of Raytheon Company, Lexington, MA, where he is involved in the development of millimeter wave HBT T/R modules. His research interests include design, fabrication, characterization, and simulation of high-frequency semiconductor devices and circuits.

Dr. Teeter is a member of Eta Kappa Nu, Phi Kappa Phi, and Tau Beta Pi.

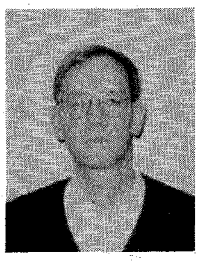

Jack R. East (M'72) received the B.S.E. degree in 1969, the M.S. degree in 1970, and the Ph.D. degree in 1986, all from the University of Michigan.

From 1974 to 1977 he was a Senior Research Associate in the Solid-State Electronics Laboratory. From 1979 to 1982 he was an Assistant Research Scientist. Currently he is an Associate Research Scientist in the Solid-State Electronics Laboratory at the University of Michigan. He has taught courses in microwave semiconductor devices and solid-state device fabrication. He is currently working in the area of fabrication and analysis of microwave solid-state devices and circuits, modeling of transport and interfaces in semiconductors, and microwave and millimeter-wave measurements.

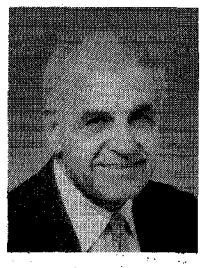

George I. Haddad received the B.S.E., M.S.E., and Ph.D. degrees in electrical engineering from the University of Michigan.

In 1958 he joined the Electron Physics Laboratory, where he was engaged in research on masers, parametric amplifiers, detectors, and electron-beam devices. From 1960 to 1969 he served successively as Instructor, Assistant Professor, Associate Professor, and Professor in the Electrical Engineering Department. In 1991 he was named the Robert J. Hiller Professor of Electrical Engineering. He served as Director of the Electron Physics Laboratory from 1968 to 1975. From 1975 to 1987 he serves as Chairman of the Department of Electrical Engineering and Computer Science. He is currently Chairman of the Department of the Electrical Engineering and Computer Science and Director of the Center for High-Frequency Microelectronics. His current research areas are microwave and millimeter-wave solid-state devices, monolithic integrated circuits, and microwave-optical interactions.

Dr. Haddad received the 1970 Curtis W. McGraw Research Award of the American Society for Engineering Education for outstanding achievements by an engineering teacher; the College of Engineering Excellence in Research Award (1985); the Distinguished Faculty Achievement Award (1986) of the University of Michigan; and the S. S. Attwood Award for excellence in engineering research, education, and administration. He is a member of Eta Kappa Nu, Sigma Xi, Phi Kappa Phi, Tau Beta Pi, and the American Society for Engineering Education. He served as Editor of the IEEE TRANSACTIONS ON MICROWAVE THEORY AND TECHNIQUES from 1968 to 1971.